Structural Changes and Chain Radius of Gyration in Cold-Drawn Polyethylene after Annealing: Small- and Wide-Angle X-ray Scattering and Small-Angle Neutron Scattering Studies

Yongfeng Men,*,† Jens Rieger,‡ Peter Lindner,§ Hans-Friedrich Enderle,⊥ Dieter Lilge,⊥ Marc O. Kristen,⊥ Shahram Mihan,⊥ and Shichun Jiang†,||

State Key Laboratory of Polymer Physics and Chemistry, Changchun Institute of Applied Chemistry, Chinese Academy of Sciences, Renmin Street 5625, 130022 Changchun, Jilin, P. R. China, BASF Aktiengesellschaft, Polymer Physics, 67056 Ludwigshafen, Germany, Institut Laue-Langevin, F-38042 Grenoble, France, Basell Polyolefine GmbH, R&D, 65926 Frankfurt, Germany, and Physikalisches Institut der Albert-Ludwigs-Universität, 79104 Freiburg, Germany

Received: May 24, 2005; In Final Form: July 6, 2005

Samples made from linear polyethylene were drawn at room temperature and subsequently annealed at high temperatures below the melting point. The structural changes of the crystalline lamellae and lamellar superstructures as well as the single chain radius of gyration were studied by means of combined small- and wide-angle X-ray scattering and small-angle neutron scattering (SANS). After drawing, the polymeric chain segments in the crystalline phase are preferentially oriented along the drawing direction with a high degree of orientation whereas the lamellae in the samples are found to be slightly sheared exhibiting oblique surfaces as evidenced by X-ray scattering. SANS indicates that the chains are highly elongated along the drawing direction. Annealing the deformed samples at temperatures where the mechanical α-process of polyethylene is active leads to a thickening of both crystalline lamellae and amorphous layers. The chains in the crystalline phase retain their high degree of orientation after annealing while the lamellae are sheared to a larger extent. In addition, there is also lateral growth of the crystalline lamellae during high-temperature annealing. Despite the structural changes of the crystalline and amorphous regions, there is no evidence for global chain relaxation. The global anisotropic shape of the chains is preserved even after prolonged annealing at high temperatures. The results indicate that the mobility of polyethylene chains—as seen, e.g., by ^{13}C NMR—is a local phenomenon. The results also yield new insight into mechanical properties of drawn PE, especially regarding stress relaxation and creep mechanisms.

I. Introduction

Linear polyethylene (LPE) is a model polymer for many fundamental studies because of its simple chemical structure. LPE normally crystallizes only partly; it assumes a semicrystalline state when being cooled from the melt. In most cases, spherulites assembled from periodically stacked crystalline lamellae with a periodicity of 20 to 50 nm are found.[1] The lamellar crystals usually have a thickness of several to tens of nanometers and a lateral size of some micrometers, as seen by electron microscopy.[1] The polymer chains are in most cases oriented parallel to the lamellar normal. Because of its large curvilinear length a single polymer passes one or several times through lamellae, forming stems that register into the crystal structure of the lamellae. The chain segments outside the lamellae form the amorphous polymeric phase. The global conformation of a single chain is preserved upon rapid crystallization implying that a single molecule must be incorporated on average into several lamellae when the radius of gyration of the single chain is large enough.[2] Although many other polymers, like polypropylene, polyamide, etc., form similar crystalline lamellar structures after solidification, LPE differs from these polymers with respect to its chain mobility in the crystalline phase. Longitudinal sliding diffusion of polyethylene chains in the crystallites results in diffusional exchange of segments of the chains between the crystalline and the amorphous phase.[3−7] Many specific physical properties of LPE, like lamellar surface melting and recrystallization,[1] high-temperature relaxation,[5,6,8] high plasticity,[9] etc., have been linked to the sliding diffusion of LPE chains in the crystallites. The sliding diffusion can be accomplished by the diffusion of a localized chain twist of 180° resembling the motion of one-dimensional solitons.[10,11] The motion of the 180° twist is a thermally activated process and is fast at elevated temperatures below the melting point of the crystalline lamellae.[3] Solid-state diffusion of paraffin molecules (e.g. of $C_{32}H_{66}$) over micrometer distances and more within hours has been observed and attributed to the mobility of the chain molecules in the crystalline phase.[12] The longitudinal mobility of chain segments in the crystalline phase might suggest that LPE chains in the solid state can be considered similarly to those in the melt state, i.e., that LPE chains are able to undergo reptational motion in the solid state though being slower than in the melt. Diffusion of PE chains in the solid state has been the major issue in studies based on mostly nuclear magnetic resonance (NMR) spectroscopy.[3,7,13]

* Address correspondence to this author. E-mail: men@ciac.jl.cn.
† Chinese Academy of Sciences.
‡ BASF Aktiengesellschaft.
§ Institut Laue-Langevin.
⊥ Basell Polyolefine GmbH.
|| Physikalisches Institut der Albert-Ludwigs-Universität.

10.1021/jp052723g CCC: $30.25
Published on Web 08/11/2005

However, NMR is only sensitive to short-range exchanges of monomeric units between the crystalline and amorphous phases. A PE chain of moderate molecular weight possesses a dimension of tens of nanometers meaning that the single chain must pass through different lamellae and amorphous regions. It is thus a priori not clear how small-scale diffusion affects long-range chain diffusion.

Due to the large difference in the scattering length of hydrogen and deuterium with regard to neutrons one can monitor single chain conformational features of tracer molecules by SANS after mixing tracer molecules of deuterated PE into the hydrogenated PE matrix.[2,14] Because SANS cannot recognize the diffusion of chains in the isotropic samples—even if there was such a process—because the shape of the chains does not change on the average, we used drawn PE to study relaxational and thus indirectly diffusional behavior of tracer polymers.

It is well-known that upon stretching, the spherulitic structure of solid PE is transformed to a fibrillar one with polymeric chains being preferentially oriented along the stretching direction.[15−19] Fibrils are composed of oriented stacks of crystalline lamellae being again separated by the amorphous phase.[20−24] The fibril thickness and thus the lateral width of the lamellae are much smaller than the original width of the lamellae in the isotropic sample. Fibrillation during stretching can be understood as a mechanically induced lamellar melting−recrystallization process.[17,25,26] This view is supported by the fact that the lamellar thickness in the fibrils depends only on the stretching temperature following similar rules as in the case of polymer crystallization from the isotropic melt.[27−34] If there were a large-scale diffusion of the chains in the drawn samples, one would expect a global relaxation of the chains that should be observable by two-dimensional SANS measurements because a global relaxation of the chains would lead to a shrinkage of the elongated chains into a more isotropic shape that would yield a different SANS pattern compared to the case of un-relaxed stretched chains.

In this work we investigate the shape changes of a single chain in a drawn LPE upon annealing at elevated temperatures below the melting point. Prior to the SANS investigation, the morphological changes in the drawn PE were studied by means of small- and wide-angle X-ray scattering (SAXS, WAXS). As will be shown in the following sections, although the dimensions of the crystalline and amorphous regions vary largely upon annealing, there is no evidence for global shape change of a single chain.

II. Experimental Section

Samples. One matrix hydrogenated LPE (h-PE) and two deuterated tracer LPEs (d-PE) with low and high molecular weight were used in this work. The molecular weight distribution of the d-PEs and the matrix h-PE is shown in Figure 1. The values of the molecular weights and the values of the radius of gyration (R_g) of the two d-PEs are included in Table 1. R_g values were obtained from SANS measurements on the isotropic mixtures and will be discussed below. The polymer mixtures consisted of 3% of d-PE in standard h-PE. The mixtures were prepared by dissolution of 0.6 g of deuterated PE and 19.4 g of the h-PE in 2 L of xylene, stabilized with 1000 ppm of Irganox 1076. The solution was kept under nitrogen atmosphere for about 2 h under reflux conditions with gentle stirring (glass flask with reflux condenser). To ensure a complete dissolution the solution was checked by visual inspection for the absence of particles or optical striae. The hot solution was then poured into a volume of 2 L of cold acetone (−78 °C, cooled with dry ice (CO_2), Erlenmeyer flask) and precipitated. The precipitate was separated on a glass frit, washed with cold acetone, and then dried in a vacuum oven at 80 °C overnight. The quality of the mixture was checked by gel permeation chromatography (GPC). Finally the irregular shaped precipitate particles were milled to a homogeneous powder (particle $d < 200\ \mu$m) at liquid nitrogen temperature in a Retsch Mill ZM1.

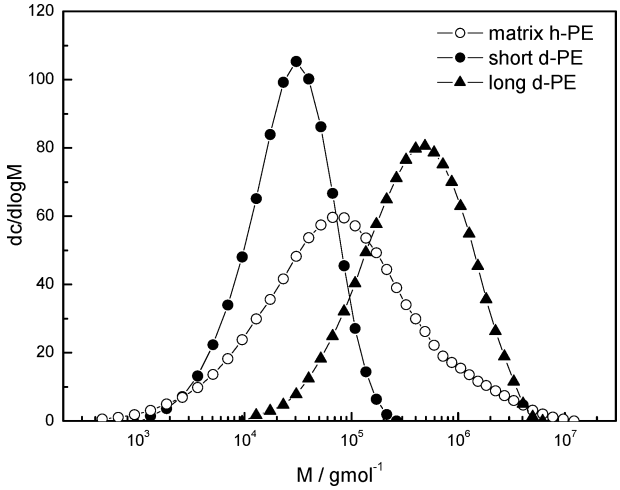

Figure 1. Molecular weight distribution of the matrix h-PE and short and long tracer d-PEs.

TABLE 1: Basic Information on the Samples: M_w and M_n Derived from GPC Measurements and R_g Values Obtained from the SANS Measurements on the Isotropic Mixtures of the d-PE Chains and the Matrix h-PE (for details see the Discussion section)

	$M_w/10^5$ gmol^{-1}	$M_n/10^5$ gmol^{-1}	R_g/nm
matrix h-PE	3.24	0.23	
short d-PE	0.41	0.18	12
long d-PE	7.13	2.19	35

The GPC of the materials was performed in a Waters 2000 GPC with 1,2,4-trichlorobenzene at 135 °C as solvent. The calibration was done with narrow and broad polyethylene standards. The software used was NTeqGPC V6 of HS-GmbH.

Films of about 0.3 mm thickness were obtained via melt pressing the dry precipitate between two pieces of aluminum foil at 160 °C for 2 min and quenching into ice water—at conditions described in the literature.[15,16,35,36] It is safe to assume that no phase separation between deuterated and hydrogenated PE chains occurred during sample preparation because the scattering data can be explained in a consistent way by using the known molar masses of the polymers. Furthermore, the procedure is the same as the one described in the literature for similar purposes.[15,16,35,36] PE samples were obtained by drawing the cut films to the natural drawn ratio (where the neck is propagated over the whole sample area) at room temperature. The macroscopic draw ratio is about 5.3. The drawn samples were then kept under stress with the aid of a metal fixing frame and annealed for 264 h at 23, 80, and 100 °C, respectively, in a vacuum oven.

Small- and Wide-Angle X-ray Scattering. SAXS and WAXS data were collected with a Nanostar AXS system of Bruker GmbH (Karlsruhe, Germany) under vacuum. The system uses an X-ray tube (Siemens) working at 40 kV and 35 mA producing Cu Kα radiation of wavelength 0.154 nm. A Göbel mirror was used to focus and enhance the X-ray intensity. The sample-to-detector distances were 650 and 92 mm for SAXS and WAXS measurements, respectively. The distances were calibrated with the scattering peaks of silver behanate. The data

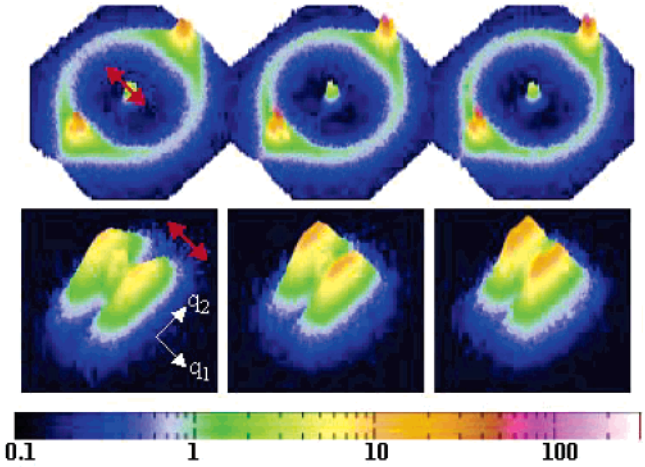

Figure 2. Small (bottom) and wide (top) angle X-ray scattering patterns of the drawn PE fiber annealed for 264 h at 23, 80, and 100 °C (from left to right). The red arrows indicate the drawing direction.

acquisition time for each pattern was 1 h. The SAXS patterns were background corrected, using the knowledge of the X-ray transmission coefficient of the samples being measured with the use of glassy carbon, which scatters X-rays intensively over the angular range of the detector. Data processing was performed with the computer program "Fit2D".[37]

Small-Angle Neutron Scattering. SANS measurements were carried out at the instrument D11 at the Institute Laue-Langevin, Grenoble. The wavelength of the neutrons was 0.6 nm with a spread in wavelength of 10%. The sample-to-detector distance was 15 m in all cases. The detector contains a 64 × 64 array of 1 cm^2 pixels. The SANS data were background corrected and normalized, using water as a standard.[38,39] The weak incoherent scattering from the hydrogenous matrix was subtracted during data processing.

III. Results and Discussion

Microstructural Changes of the Drawn LPE upon Annealing. The size and the orientation of crystalline lamellae in the samples were first characterized by means of SAXS and WAXS. The results are presented in Figure 2. All WAXS patterns indicate a high degree of orientation of the polymeric crystallites. The peaks in the WAXS patterns are assigned to the crystallographic 110 and 200 planes of the orthorhombic form of polyethylene. The peaks in the SAXS data originate from the regular stacking of the crystalline lamellae in the fibrils. It is evident from Figure 2 (top) that the PE chains in the crystallites are oriented along the stretching direction. On annealing, the scattering intensities in both the WAXS and the SAXS data increase. The shape of the WAXS pattern remains essentially unchanged indicating that the high orientation of the chains in the crystallites is preserved whereas the shape of the SAXS pattern varies upon annealing meaning that there is a change in the arrangement of the scattering objects, i.e., the lamellae. The dimensions of the crystallites perpendicular to the crystallographic 110 and 200 planes were obtained using the Scherrer equation:[40]

$$L_{hkl} = \frac{K\lambda}{\beta_0 \cos\theta} \cong \frac{2\pi}{\Delta q_{hkl}} \qquad (1)$$

where L_{hkl} is the dimension of the crystallites perpendicular to the planes *hkl*, K is a constant and is set to unity, λ is the wavelength of the X-rays, β_0 is the width at half-maximum of the diffraction profile in radians, 2θ is the scattering angle, and Δq_{hkl} is the width at half-maximum of the diffraction profile (in nm^{-1}). We evaluated the dimensions of L_{110} and L_{200} using the one-dimensional intensity distribution profiles along the equatorial direction of the WAXS patterns. The width at half-maximum of the diffraction peaks of the 110 and 200 planes (Δq_{110} and Δq_{200}) and the dimensions L_{110} and L_{200} are given in Table 2. It must be mentioned that due to the limited pixel size of the X-ray detector (100 μm) 10% of uncertainty must be considered in the calculation. Even though the effect of annealing on the crystallite size L_{110} and L_{200} is clearly seen, the lateral size of the crystalline lamellae perpendicular to the 110 and 200 crystallographic planes increases by 2 to 3 nm, i.e., up to 30%, as the annealing temperature increases from 23 to 100 °C. The size of the crystallites along the chain direction cannot be obtained from the WAXS data because of the lack of a crystallographic 001 peak. This value, however, can be derived from the SAXS data, as will be shown below.

Before discussing the thickness of the crystalline lamellae and of the interlamellar amorphous zones, we consider the lateral dimensions and the orientation of the crystalline lamellae by analyzing the SAXS data. In the SAXS patterns, the scattering vectors along and perpendicular to the stretching direction are defined as q_1 and q_2, respectively. The characteristic feature of the SAXS patterns of the stretched samples is that the scattering intensity is concentrated along two straight segments perpendicular to the stretching direction on both sides of the beam stop. The samples annealed at 80 and 100 °C exhibit a four-point SAXS pattern. This is better seen in an azimuthal scan across the lamellar peak along q_2, cf. Figure 3. A four-point pattern is indicative of a shearing or tilting of the orientated lamellae[41] or a checkerboard-like arrangement of crystallites.[42] The latter case is not considered further since there is no indication for a correlated checkerboard-like arrangement of crystalline lamellae from, e.g., electron microscopic investigations. Since there is no evidence for an arc-like distortion of the lamellar peaks, it is reasonable to extract from the data in Figure 3 the angle of inclination of the crystal surfaces and the size of the lamellae.[42] The intensity distribution along q_2 was fitted with two Lorentz functions as shown in the inset of Figure 3. The width of the resulting Lorentz function (Δq_2) is directly related to the lateral size of the lamellae ($L_{SAXS} = 2\pi/\Delta q_2$) and the separation of the centers of the two Lorentz functions ($\Delta\chi$) is assigned to the lamellar shearing.[42] On the basis of a purely geometric consideration, the angle (Φ) between the normal of the lamella and the fiber axis was obtained with the following equation:

$$\Phi = \tan^{-1}\frac{\Delta\chi}{2q_{1,\max}} \qquad (2)$$

where $q_{1,max}$ is the lamellar peak position along q_1 at $q_2 = 0$. Values for Δq_2, L_{SAXS}, $\Delta\chi$, and Φ are included in Table 2. The values of L_{SAXS} are somewhat larger than those obtained from WAXS data, but the trend when varying the annealing conditions agrees with the one extracted from the WAXS measurements, namely, a lateral growth of the lamellar crystallites induced by annealing. The discrepancy between the values derived from the WAXS and SAXS data is due to the fact that WAXS measures the extension of the crystalline lattices whereas SAXS is sensitive to the density difference between the phases.

The respective average thickness of lamellar and amorphous regions along the stretching direction can be obtained by considering the scattering intensity distribution along the q_1 direction. A one-dimensional intensity distribution was obtained

TABLE 2: Microstructural Information and Chain Dimensions for PE Fibers Annealed for 264 h at Different Temperatures (T_a)[a]

T_a/ °C	Δq_{110}/ nm^{-1}	Δq_{200}/ nm^{-1}	L_{110}/ nm	L_{200}/ nm	Δq_2/ nm^{-1}	L_{SAXS}/ nm	$\Delta\chi$/ nm^{-1}	Φ/ deg	d_{ac}/ nm	d_a/nm	d_c/ nm	$\phi_{l,c}$	$R_{g,1}$[b]/ nm	$R_{g,2}$[b]/ nm	R_{g2}[c]/ nm
23	0.63	0.63	10	10	0.60	11	0.21	15	15	6	9	0.60	47.3	9.5[d]	14.3
80	0.52	0.57	12	11	0.42	15	0.29	21	17	7	10	0.59	46.5	9.9[d]	15.1
100	0.48	0.52	13	12	0.36	17	0.32	27	20	8	12	0.60	44.8	10.2[d]	15.2

[a] Width of the 110 and 200 peaks from WAXS (Δq_{110} and Δq_{200}), dimensions of crystallites measured along the 110 and 200 planes (L_{110} *and* L_{200}), width of the SAXS lateral intensity distribution (Δq_2), lamellar lateral size (L_{SAXS}), separation of the two lamellar peaks along q_2 ($\Delta\chi$), angle between the normal of lamellae surfaces and the fiber axis (Φ), long spacing (d_{ac}), amorphous layer thickness (d_a), lamellar thickness (d_c) derived from SAXS, radius of gyration of single tracer chains along and perpendicular to the stretching direction ($R_{g,1}$ and $R_{g,2}$) [b] For the short tracer polymer. [c] For the long tracer polymer. [d] Values suffer from large scatter and serve only as an indicator (see the discussion in the text).

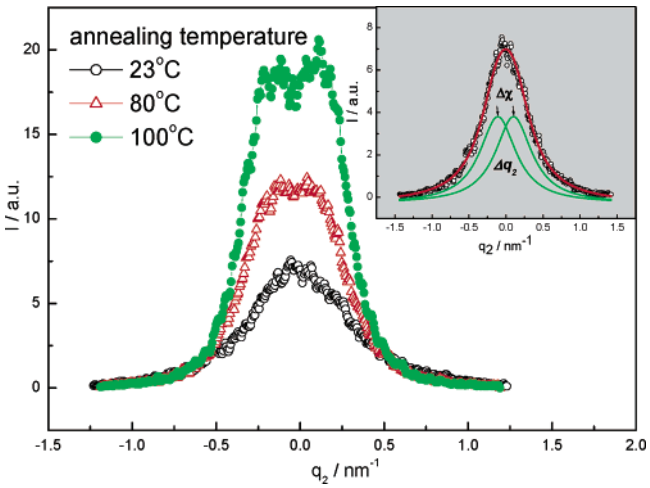

Figure 3. SAXS: azimuthal scan of the lamellar peaks along q_2. The inset shows the fit procedure used for the evaluation of the lateral size and the inclination angle of lamellae (see text for details).

by integrating the intensity at each q_1 for a certain range of q_2 as follows:

$$I(q_1) = \int_{q_{2,a}}^{q_{2,b}} I(q_1,q_2)\, dq_2 \qquad (3)$$

where $q_{2,a}$ and $q_{2,b}$ are selected in such a way that the lamellar scattering peak covers the range of the integration. It must be mentioned that the above data treatment makes sense only if the lamellar scattering intensity is not arc-shaped.[42] Curves of $I(q_1)$ of samples annealed at different temperatures are shown in Figure 4. The long spacing, d_{ac} ($d_{ac} = d_a + d_c$, where d_a and d_c are the average thickness of the amorphous and the crystalline layers, respectively, measured along the drawing direction), of the samples was obtained from the peak position of $I(q_1)$ according to Bragg's law:

$$d_{ac} = \frac{2\pi}{q_{1,max}} \qquad (4)$$

It is seen that the long spacing d_{ac} increases with increasing annealing temperature, cf. Table 2. The average thickness of the amorphous and crystalline regions measured along the drawing direction can be derived from the one-dimensional correlation function $K(z)$ as follows:[1,42−45]

$$K(z) = \frac{\int_0^\infty I(q_1)\cos(q_1 z)\, dq_1}{\int_0^\infty I(q_1)\, dq_1} \qquad (5)$$

where z denotes the drawing direction. In the above consideration, no multiplication q_1^2 to $I(q_1)$ is performed because of the anisotropic orientation of the lamellae in the samples.[1,42,45,46]

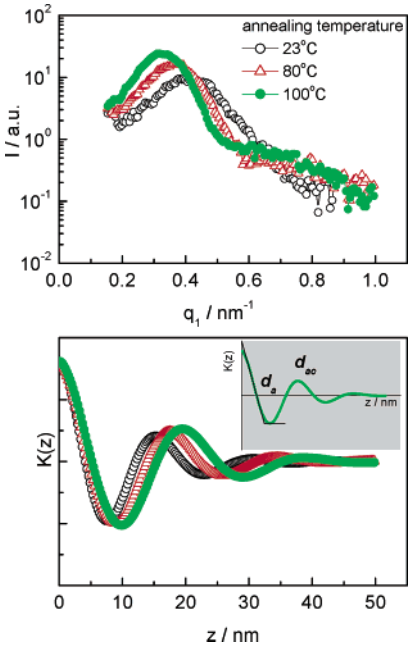

Figure 4. SAXS: one-dimensional scattering intensity distribution along the stretching direction (top) and its correlation function (bottom). The maximum position in the top curves indicates the long spacing (d_{ac}) of the lamellar stacks. The long spacing (d_{ac}) and the average amorphous layer thickness (d_a) can be obtained from the correlation function as shown in the inset of the bottom figure.

The resultant correlation functions for the three samples investigated are shown in the bottom plot of Figure 4. The inset of Figure 4 shows how the average thickness of the amorphous layers (d_a) and of the long spacing (d_{ac}) are obtained.[1] It must be mentioned that it is impossible to decide whether it is the amorphous or the crystalline thickness that is read out from the correlation function without prior knowledge of the crystallinity.[1] However, the sample used in the present study was a high-density polyethylene that under the given conditions ensures the assignment of the small value to the average thickness of the amorphous layers. The average thickness of the crystalline lamellae can be obtained with the relation $d_c = d_{ac} - d_a$. The long spacing obtained from the correlation function is identical with that obtained from the intensity distribution data $I(q_1)$ using Bragg's law directly. Knowing the average thickness of the amorphous and crystalline layers, the linear crystallinity ($\phi_{l,c} = d_c/d_{ac}$) of the system was calculated.[47] The values of d_a, d_c, d_{ac}, and $\phi_{l,c}$ for samples annealed at different temperatures are included in Table 2. Upon annealing, the average thickness of both the amorphous phase and the crystalline lamellae increases. But these changes are correlated in such a way that the linear crystallinity along the stretching direction remains essentially constant. The increase in the long spacing and in the thickness of the crystalline lamellae is indicative for a melting of thin

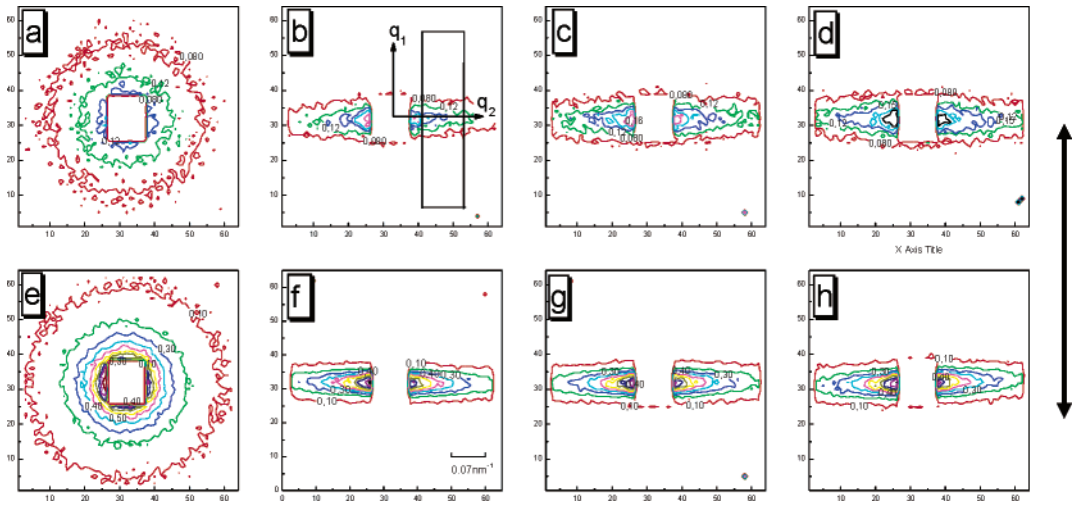

Figure 5. SANS patterns of the isotropic PE and drawn fiber containing short (top) and long tracer polymers (bottom): isotropic samples (a, e) and fibers after annealing for 264 h at 23 (b, f), 80 (c, g), and 100 °C (d, h). The arrow on the right side of the patterns indicates the stretching direction.

lamellae, which have formed between thicker lamellae, followed by a recrystallization of the freed polymeric segments onto both the longitudinal and the lateral surfaces of the adjacent lamellae.

The Shape of a Single Chain. The results of the WAXS and SAXS measurements have shown that the microscopic structure of the drawn PE changes during annealing. It was also shown that the average thicknesses of the crystalline and the amorphous layers are about 10 nm being significantly smaller than the radius of gyration of a high molecular weight tracer PE chain but comparable with the radius of gyration of the shorter ones. It is thus interesting to investigate the global shape changes of single chains after drawing and annealing. The global shape of single chains was measured with SANS on hydrogenated PE samples mixed with two different tracer d-PE molecules, namely, short and long d-PEs. The undeformed samples were investigated by SANS to obtain the molecular dimension in the isotropic state. Patterns a and e in Figure 5 present SANS contour plots from samples with short and long tracer molecules, respectively. From these plots it is seen that the sample with long tracer molecules scatters much stronger than the one with short ones. This is expected since the neutron scattering intensity ($I(q)$) is related to the length of the tracer molecules as follows:[14,48−50]

$$I(q) = (b_D - b_H)^2 x(1-x) N z^2 P(q) \qquad (6)$$

where b_D and b_H are the neutron scattering lengths of hydrogenated and deuterated monomers, x is the fraction of one component, N is the number of tracer molecules, z is the average number of monomers per tracer molecule, and $P(q)$ is the structure factor of a single chain. For polymers of sufficient length $P(q)$ is approximately given by the Debye equation:[51]

$$P(q) = \frac{2}{\lambda^2}[\lambda - 1 + e^{-\lambda}] \qquad (7)$$

with $\lambda = q^2 R_g^2$, where R_g is the radius of gyration of the tracer molecule. Because the total number of monomers of the tracer chains is the same in both samples the scattering intensity is proportional to z (eq 6) and thus proportional to the molecular weight of the tracer molecules. To calculate the values of R_g of the two different tracer molecules, the scattering patterns for undeformed samples were averaged over all directions at constant q resulting in one-dimensional scattering intensity

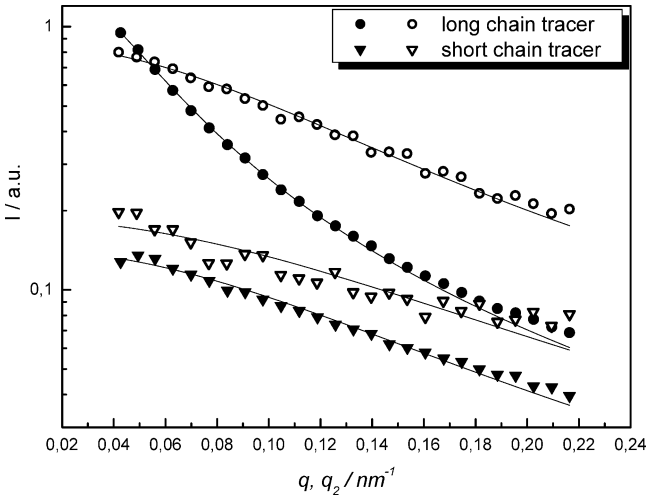

Figure 6. SANS: one-dimensional scattering intensity distributions of isotropic (solid symbols) and stretched PE (hollow symbols). The scattering intensity of the stretched samples was taken from the two-dimensional data sets by choosing rectangles perpendicular to the stretching direction and passing through the beam center. The incoherent scattering from the hydrogenated LPE matrix was subtracted from the data. Curves were fitted with the Debye structure factor of Gaussian chains; the solid lines denote the results of the fitting procedure.

curves ($I(q)$ vs q): black symbols in Figure 6. These data were fitted with eq 6 by combining all pre-factors in front of $P(q)$ as a single parameter, which yields two parameters left for fitting, namely, the pre-factor and the radius of gyration. The results of such a fit are included in Figure 6 (solid lines). As is seen in Figure 6 the fitting for the long tracer chain is good for scattering vectors $q < 0.18$ nm^{-1} indicating Gaussian behavior of the single chain in the solid PE at larger length scales. From this fitting a radius of gyration of 35 nm is derived. Though the application of the Debye equation is somewhat questionable in the case of the sample containing short tracer molecules, the fitting was performed formally and yields a radius of gyration for the short tracer molecules of 12 nm. The R_g values for the short and long tracer molecules are in agreement with those obtained by Sadler and Barham.[15,16]

On stretching, the distribution of the chain segments is no longer isotropic due to the preferential orientation of the chains. Consequently, the neutron scattering patterns of the stretched samples are anisotropic as seen in Figure 5 (patterns b and f).

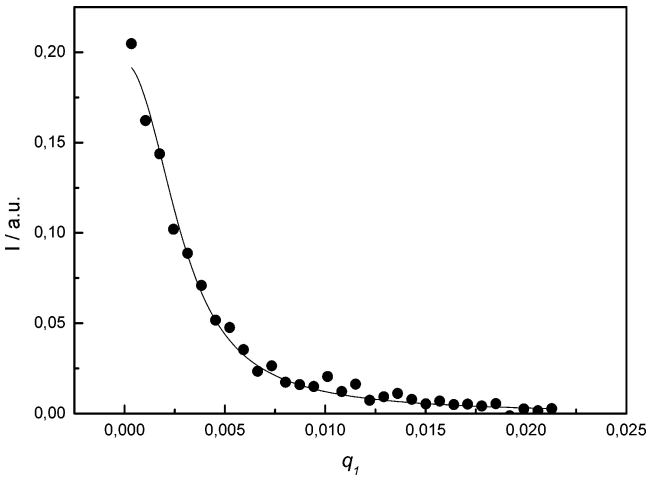

Figure 7. SANS intensity distribution along the stretching direction as derived by averaging the intensity over appropriate ranges of q_2 at each q_1. The solid line shows the result of a fit with the Debye equation.

The scattering intensity distribution along the equator can be used to derive the dimension of the tracer chains perpendicular to the stretching direction.[15,16] q_1 is parallel to the stretching direction and q_2 points in the equatorial direction. The hollow symbols in Figure 6 show the scattering intensity as a function of q_2 for the two stretched samples with tracer molecules of different lengths. These data were obtained from the two-dimensional data sets by using rectangular cuts along the equator passing through the beam center. The Debye equation was used again to fit the curves and to obtain the dimensions of the molecules perpendicular to the stretching direction. $R_{g,2}$ values of 9.5 and 14.3 nm for the short and long tracer molecules were obtained. For the long tracer molecules the value indicates a molecular drawn ratio of 6, which is slightly larger ($\lambda = 6$ compared to 5.3) than expected for affine deformation of the chains with macroscopic deformation, whereas for the short tracer molecules the value is larger than expected for affine deformation, which would yield 5.6 nm instead of 9.5 nm. However, the data of the sample containing short tracer chains exhibit comparatively large scatter thus reducing the reliability of the R_g value for the short tracer molecules. To obtain additional information the scattering intensity distribution along the meridional direction (q_1) was considered. The intensity was averaged along q_2 at each q_1 value over certain ranges as indicated in pattern b of Figure 5. The width of the rectangle does not influence the shape of the curve $I(q_1)$[15,16] so that it is possible to average the intensity over a large range to obtain better statistics. The resultant curve of $I(q_1)$ is shown in Figure 7. Fitting this curve with the Debye equation results in a value of 47.3 nm for the radius of gyration along the stretching direction $R_{g,1}$. If the short tracer molecules deform affinely with respect to the macroscopic deformation, $R_{g,1}$ should have a dimension of 63.6 nm. The same procedure of deriving $R_{g,1}$ cannot be applied to the scattering pattern of the samples containing long tracer molecules because of the limited resolution of the setup. At first sight, it appears confusing that the tracer molecules do not follow the macroscopic deformation affinely. One possible explanation lies in the heterogeneous strain distribution in the system at late stages of the deformation. After fibrillation, the macroscopic deformation can be accomplished by slippage of the fibrils past each other. The molecules inside the fibrils are no longer stretched despite the macroscopic drawing. But the chains connecting adjacent fibrils are stretched farther during slippage of the fibrils. This consideration makes sense because it is evident that the dimension of the fibrils in drawn samples is comparable to that of the stretched short tracer molecule but smaller than that of long tracer molecule. We have no direct observation of the length of the fibrils in our system but it was found that the fibrils in high modules PE fibers have a length in the range of 130 to 330 nm.[52] It should be mentioned that the high modules PE fibers are produced either via gel-spinning or by ultra-drawing of low entanglement density single-crystal PE mats.[52] Both processes are supposed to yield more perfect fibrils than the ones found in the samples used in this work. Thus, the fibrils in the drawn PE in the present case must be much shorter than the stretched long molecules. This implies that the long chains interconnect the fibrils in the longitudinal direction as well. The above explanation coincides with the observation of a smaller molecular draw ratio in the case of short tracer chains and a larger molecular draw ratio of long tracer chains compared to the macroscopic deformation.

It was shown above that the microscopic structure of the drawn PE samples underwent large changes after annealing at 80 and 100 °C. We now consider the single chain shape changes after high-temperature annealing. In Figure 5 patterns c and g represent the SANS counter plots for the samples annealed at 80 °C and patterns d and h are for the samples annealed at 100 °C. In both cases, no effects of annealing on the single chain scattering, i.e., single chain shape in the respective range of length scales as given by the q-range, are seen. The short chains as well as the long chains retain their global anisotropic shape after high-temperature annealing. Similar data treatment as discussed above was used to obtain the corresponding R_g values of the short and long chains after annealing. The values are included in Table 2. The R_g values of both short and long chains show only slight changes after annealing. These small changes are assumed not to be a result of the sliding diffusion of the chains but to be induced by the melting of defective crystallites during annealing. The following points speak in favor of this interpretation: first, it must be assumed that a certain shrinkage of the stretched chains is due to the fact that segments close to the end of the polymer chain will relax upon local melting of the lamellae during annealing; second, if chain sliding diffusion was active, one would expect a distinct change in the chain conformation between samples annealed at 80 and 100 °C, such a change is not observed. Therefore, it is safe to state that on the time scale of the present study no large-scale relaxation (mediated by diffusional processes) of the PE chains in the drawn sample is seen.

Structural Model. Acknowledging SAXS, WAXS, and SANS results, the following structural model for freshly prepared and annealed drawn PEs is proposed. Figure 8 shows the schematic representation of the microscopic structure in a drawn PE; only representative tracer molecules and crystalline lamellae are shown. On the left-hand side of Figure 8 a freshly drawn PE shows a broad thickness distribution of the crystalline lamellae. The polymer chains in the crystallites are oriented along the stretching direction but the lamellar normal is inclined somewhat with respect to the stretching direction. The polymer chains are stretched along the fiber axis. During high-temperature annealing below the melting point some defective crystallites melt and recrystallization occurs both along the chain direction (crystallite thickening) and on the lateral edges of the existing lamellae (Figure 8 right-hand side). The orientation of the chains in the crystallites is preserved but the lamellae surfaces are inclined further (cf. Table 2). This further inclination might be explained by assuming an uneven stress distribution across the surfaces stemming from the stressed state of the

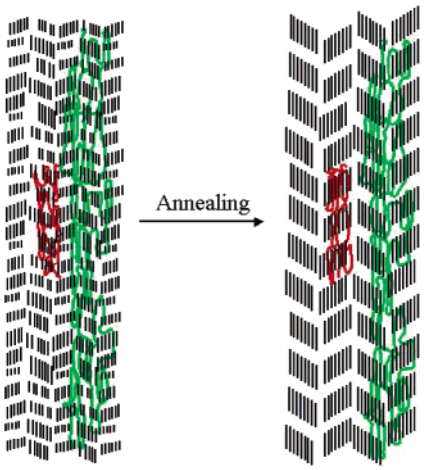

Figure 8. Schematic representation of the structural evaluation of a drawn PE sample after high-temperature annealing (below the melting point). The red and green chains represent the shape of the short and long chains before and after annealing. Only representative tracer molecules and crystalline lamellae are shown.

polymer chains involved. Some of the local stresses can be released by longitudinal diffusion leading to corrugated and tilted surfaces. The resulting structure exhibits thicker lamellae and amorphous regions than the original material. The thickening of the crystalline lamellae is a result of the high mobility of PE chains due to sliding diffusion in the crystalline state. However, this diffusional process is active only locally, the global anisotropic shape of the molecular chain is not affected.

Mechanical Consequence. The above finding that polyethylene chains are essentially fixed in the drawn state, even at elevated temperatures, has important consequences for the understanding of the mechanical properties of drawn PEs and PE components. Especially, the mechanism of stress relaxation and creep of drawn PE can be understood better according to the above results. The occurrence of chain disentanglements during stress relaxation is excluded because the chains are fixed globally in stacks of lamellae (fibrils). Yet, considerable stress relaxation is observed during annealing, e.g. in mechanical testing. One possible route to relax the stress of a drawn orientated sample is the slippage of fibrils past each other as has been found in the case of polyamide 6 fibers.[53] This slippage is assumed to be due to the relaxation of stretched chains connecting adjacent fibrils. This relaxational process is not seen in the SANS data because the fraction of these connecting chains seems to be considerably smaller than the fraction of chains being fixed in the stacks of lamellae in the fibrils.

IV. Conclusion

We have investigated the evolution of the microscopic crystalline and amorphous structure and the single chain shape of drawn PEs at high-temperature annealing below the melting point by means of small- and wide-angle X-ray scattering and small-angle neutron scattering. Although the thicknesses of both crystalline lamellae and amorphous regions increase during high-temperature annealing (well above the α-relaxation temperature of PE, implying a high internal mobility of PE chains in the crystalline phase), no global shape change of single stretched chains has been observed. It appears that the sliding diffusion of PE chain in the crystalline phase is a localized phenomenon restricted to adjacent lamellae and amorphous regions only—at least at the temperature and the time scales investigated. The results are important for understanding the mechanical response of PE fibers, especially the stress relaxation mechanism. Since the chains are fixed globally, the stress relaxation cannot be caused by the disentangling of the orientated polymeric chains but must be attributed to the reorganization and shearing of the crystalline lamellae assisted by the high mobility of the chains in the crystallites.

Acknowledgment. We thank Dr. R. E. Ghosh for his help on SANS data treatments and Prof. G. Strobl for helpful discussions.

References and Notes

(1) Strobl, G. *The Physics of Polymers*, 2nd ed.; Springer: Berlin, Germany, 1997.
(2) Kaji, K. In *Applications of Neutron Scattering to Soft Condensed Matter*; Gabrys, B. J., Ed.; Gordon and Breach Science Publisher: New York, 2000; p 107.
(3) Schmidt-Rohr, K.; Spiess, H. W. *Macromolecules* **1991**, *24*, 5288.
(4) Olf, H. G.; Peterlin, A. *J. Polym. Sci. Part A2* **1970**, *8*, 771.
(5) Boyd, R. H. *Polymer* **1985**, *26*, 323.
(6) Boyd, R. H. *Polymer* **1985**, *26*, 1123.
(7) Klein, P. G.; Driver, M. A. N. *Macromolecules* **2002**, *35*, 6598.
(8) Men, Y. F.; Rieger, J.; Enderle, H.-F.; Lilge, D. *Macromolecules* **2003**, *36*, 4689.
(9) Hu, W. G.; Schmidt-Rohr, K. *Acta Polym.* **1999**, *50*, 271.
(10) Zubova, E. A.; Balabaev, N. K. *J. Nonlinear Math. Phys.* **2001**, *8* (*Suppl.*), 305.
(11) Balabaev, N. K.; Gendelman, O. V.; Manevitch, L. I. *Phys. Rev. E* **2001**, *64*, 036702.
(12) Ungar, G.; Keller, A. *Colloid Polym. Sci.* **1979**, *257*, 90.
(13) Robertson, M. B.; Ward, I. M.; Klein, G.; Packer, K. J. *Macromolecules* **1997**, *30*, 6893.
(14) Higgins, J. S.; Benoit, H. C. *Polymers and Neutron Scattering*; Oxford University Press: New York, 1994.
(15) Sadler, D. M.; Barham, P. J. *Polymer* **1990**, *31*, 36.
(16) Sadler, D. M.; Barham, P. J. *Polymer* **1990**, *31*, 46.
(17) Men, Y. F.; Rieger, J.; Strobl, G. *Phys. Rev. Lett.* **2003**, *91*, 095502.
(18) Belbeoch, D. B.; Guinier, A. *Makromol. Chem.* **1959**, *31*, 1.
(19) Butler, M. F.; Donald, A. M. *Macromolecules* **1998**, *31*, 6234.
(20) Hess, K.; Kiessig, H. *Naturwissenschaften* **1943**, *31*, 171.
(21) Statton, W. O. *J. Polym. Sci.* **1958**, *28*, 423.
(22) Mandelkern, L.; Worthington, C. R.; Posner, A. S. *Science* **1958**, *127*, 1052.
(23) Posner, A. S.; Mandelkern, L.; Worthington, C. R.; Diorio, A. F. *J. Appl. Phys.* **1960**, *31*, 536.
(24) Fischer, E. W.; Schmidt, G. F. *Angew. Chem.* **1962**, *74*, 551.
(25) Men, Y.; Strobl, G. *Chin. J. Polym. Sci.* **2002**, *20*, 161.
(26) Men, Y.; Strobl, G. *Macromolecules* **2003**, *36*, 1889.
(27) Balta-Calleja, F. J.; Peterlin, A. *J. Macromol. Sci., Phys.* **1970**, *B4*, 519.
(28) Farrell, C. J.; Keller, A. *J. Mater. Sci.* **1977**, *12*, 966.
(29) Peterlin, A.; Corneliussen, R. *J. Polym. Sci. Part A2* **1968**, *6*, 1273.
(30) Peterlin, A. *J. Polym. Sci.* **1967**, *C18*, 123.
(31) Peterlin, A.; Balta-Calleja, F. J. *Colloid Polym. Sci.* **1970**, *242*, 1093.
(32) Peterlin, A.; Meinel, G. *Makromol. Chem.* **1971**, *142*, 227.
(33) Meinel, G.; Peterlin, A. *Colloid Polym. Sci.* **1970**, *242*, 1151.
(34) Corneliussen, R.; Peterlin, A. *Makromol. Chem.* **1967**, *105*, 193.
(35) Coutry, S.; Spells, S. J. *Polymer* **2003**, *44*, 1949.
(36) Coutry, S.; Spells, S. J. *Polymer* **2002**, *43*, 4957.
(37) Hammersley, A. *Computer Program Fit2D*, version V12.012; ESRF, 1998.
(38) Lindner, P. *J. Appl. Crystallogr.* **2000**, *33*, 807.
(39) Ghosh, R. E.; Egelhaaf, S. U.; Rennie, A. R. *A Computing Guide for Small-Angle Scattering Experiments*; Institut Laue Langevin: Grenoble, France, 1998.
(40) Alexander, L. E. *X-ray Diffraction Methods in Polymer Science*; John Wiley & Sons Inc.: New York, 1979.
(41) Crist, B. *J. Appl. Crystallogr.* **1979**, *12*, 27.
(42) Murthy, N. S.; Bednarczyk, C.; Moore, R. A. F.; Grubb, D. T. *J. Polym. Sci. Part B*: *Polym. Phys.* **1996**, *34*, 821.
(43) Strobl, G. R.; Schneider, M. J. *J. Polym. Sci. Polym. Phys.* **1980**, *18*, 1343.
(44) Strobl, G. R.; Schneider, M. J.; Voigt-Martin, I. G. *J. Polym. Sci. Polym. Phys.* **1980**, *18*, 1361.
(45) Glatter, O.; Kratky, O. *Small-Angle X-ray Scattering*; Acdemic Press: London, UK, 1982.
(46) Crist, B.; Morosoff, N. *J. Polym. Sci. Polym. Phys.* **1973**, *11*, 1023.

(47) Heck, B.; Hugel, T.; Iijima, M.; Sadiku, E.; Strobl, G. *New J. Phys.* **1999**, *1*, art. no. 17.

(48) Cotton, J.-P.; Decker, D.; Benoit, H. C.; Farnoux, B.; Higgins, J. S.; Jannink, G.; Ober, R.; Picot, C.; des Cloizeaux, J. *Macromolecules* **1974**, *7*, 863.

(49) Daoud, M.; Cotton, J. P.; Farnoux, B.; Jannink, G.; Sarma, G.; Benoit, H. C.; Duplessix, C.; Picot, C.; de Gennes, P. G. *Macromolecules* **1975**, *8*, 804.

(50) Akcasu, A.; Summerfield, G. C.; Jahshan, S. N.; Han, C. C.; Kim, C. Y.; Yu, H. *J. Polym. Sci. Polym. Phys.* **1980**, *18*, 863.

(51) Debye, P. *J. Phys. Colloid Chem.* **1947**, *51*, 18.

(52) Grubb, D. T.; Prasad, K. *Macromolecules* **1992**, *25*, 4575.

(53) Rieger, J. In *Neutrons, X-rays and Light Scattering Methods Applied to Soft condensed Matter*; Lindner, P., Zemb, Th., Eds.; North-Holland: Amsterdam, The Netherlands, 2002; p 481.